Biogeosciences Discuss., 10, 111–155, 2013
www.biogeosciences-discuss.net/10/111/2013/
doi:10.5194/bgd-10-111-2013

Biogeosciences Discussions

Satellite views of seasonal and inter-annual variability of phytoplankton blooms in the eastern China seas over the past 14 yr (1998–2011)

X. Q. He[1,4,*], Y. Bai[1], D. L. Pan[1], C.-T. A. Chen[2,4], Q. Chen[3], D. F. Wang[1], and F. Gong[1]

[1]State Key Laboratory of Satellite Ocean Environment Dynamics, Second Institute of Oceanography, State Oceanic Administration, Hangzhou, China
[2]Institute of Marine Geology and Chemistry, National Sun Yat-sen University, Kaohsiung, Taiwan
[3]Department of Environment Resources Management and City Planning, Zhejiang Gongshang University, Hangzhou, China
[4]Department of Ocean Science and Engineering, Zhejiang University, Hangzhou, China
[*]now at: Hangzhou, China

Received: 14 December 2012 – Accepted: 18 December 2012 – Published: 4 January 2013

Correspondence to: X. Q. He (hexianqiang@sio.org.cn) and
C.-T. A. Chen (ctchen@mail.nsysu.edu.tw)

Published by Copernicus Publications on behalf of the European Geosciences Union.

BGD
10, 111–155, 2013

Abstract

The eastern China seas are one of the largest marginal seas in the world, where high primary productivity and phytoplankton blooms are often observed. However, to date, little is known about the spatial and temporal variability of phytoplankton blooms in these areas due to the difficulty of the monitoring of bloom events by field measurement. In this study, 14-yr time series of satellite ocean color data from the Sea-Viewing Wide Field-of-view Sensor (SeaWiFS) and the Moderate Resolution Imaging Spectroradiometer (MODIS) onboard the Aqua satellite have been used to investigate the seasonal and inter-annual variability and long-term changes of phytoplankton blooms in the eastern China seas.

We validated and calibrated the satellite-derive chlorophyll concentration in the eastern China seas based on extensive data sets from two large cruises. Overestimation of satellite-derive chlorophyll concentration caused by high water turbidity was found to be less than 10 $\mu g\,L^{-1}$. This level can be used as a safe threshold for the identification of a phytoplankton bloom in a marginal sea with turbid waters. Annually, blooms mostly occur in the Changjiang Estuary and along the coasts of Zhejiang. The coasts of the northern Yellow Sea and Bohai Sea also have high-frequency blooms. The blooms have significant seasonal variation, with most of the blooms occurring in the spring (April–June) and summer (July–September). This study revealed a doubling in bloom intensity in the Yellow Sea and Bohai Sea during the past 14 yr (1998–2011), yet surprisingly, there has been no decadal increase or decrease of bloom intensity in despite of significant inter-annual variation in the Changjiang Estuary. The time series in situ datasets show that both the nitrate and phosphate concentrations increase more than twofold from 1998 to 2005. This might be the reason for the doubling of bloom intensity in the Yellow Sea and Bohai Sea. In addition, the ENSO and PDO can affect the inter-annual variation of bloom intensity in the eastern China seas.

BGD

10, 111–155, 2013

1 Introduction

The eastern China seas, including the East China Sea (ECS), Yellow Sea (YS) and Bohai Sea (BS), are one of the largest marginal seas in the world (Fig. 1a). It receives a tremendous amount of fresh water and suspended sediments from rivers, including two of the largest rivers in the world, namely, the Changjiang (Yangtze River) and Huanghe (Yellow River) (Liu et al., 2010a). The Changjiang provide 90 % of the total riverine water discharge and sediment input to the ECS (Zhang et al., 2007). The annual mean discharge of the Changjiang is 29 300 $m^3 s^{-1}$, with 70 % of the total annual runoff occurring during the flood season from May to October (Wang et al., 2010). Due to the sediment carried by rivers, the eastern China seas are among the most turbid ocean regions in the world (Shi and Wang, 2010).

The eastern China seas are one of the most productive areas in the North Pacific owing to the abundant nutrients from river discharge and incursion of the Kuroshio subsurface water on the shelf (Chen et al., 1995; Chen, 1996; Chen and Wang, 1999). The modeled annual mean primary production over the entire ECS shelf is up to 441 mg C $m^2 d^{-1}$ (Liu et al., 2010b), and episodic phytoplankton blooms are often observed in the eastern China seas (Hyun and Kim, 2003; Furuya et al., 2003; Hu et al., 2004; Son et al., 2006; Tang et al., 2006; Isobe and Matsuno, 2008; Zhao et al., 2011). Many studies using cruise data have examined the distributions of chlorophyll concentration (chl *a*) and primary production in the ECS (Gong et al., 1996, 2000, 2003, 2006; Hama et al., 1997; Chen et al., 2001, 2004; Kim et al., 2009). However, due to the limited field investigation, there are not sufficient data collected by traditional sampling methods to assess the spatial and temporal dynamics of chl *a* distributions.

Satellite ocean color data have already been used to investigate the spatial and temporal variability of chl *a* in all the eastern China seas. Ning et al. (1998) and Tang et al. (1998) had studied monthly variations of pigment concentrations measured by the Coastal Zone Color Scanner (CZCS) onboard the Nimbus-7 satellite. Kiyomoto et al. (2001) examined the seasonal and spatial distributions of chl *a* and suspended

BGD
10, 111–155, 2013

particulate matter concentration using satellite data from the CZCS and OCTS (Ocean Color and Temperature Scanner) on board the Advanced Earth Observing Satellite (ADEOS). However, satellite data generally overestimate chl *a* in turbid coastal waters. The operational satellite retrieval algorithm for chl *a* uses the blue-green band ratio of remote sensing reflectance, with low ratios corresponding to high chl *a*. Additional terrestrial detritus and colored dissolved organic matter (CDOM) could significantly increase the water's absorption coefficient and decrease the remote sensing reflectance at the blue band, while it enhances the particulate backscattering coefficient and increases the remote sensing reflectance at the green band, and hence the chl *a* is overestimated by blue-green band ratio algorithm. Recently, using 8 yr (2002–2009) of observations from the Moderate Resolution Imaging Spectroradiometer (MODIS) onboard the Aqua satellite, Shi and Wang (2012) developed climatology of seasonal distributions of satellite-derive chl *a* in the eastern China seas. However, they did not present the inter-annual variation since of the significant uncertainty in satellite-derive chl *a* occurring in these regions. Meanwhile, Yamaguchi et al. (2012) also investigated a seasonal climatology of satellite-derive chl *a* in the YS and ECS using 10 yr (September 1997 to October 2006) of chl *a* data observed by the Sea-Viewing Wide Field-of-view Sensor (SeaWiFS). Because of the significant overestimation of satellite-derive chl *a* in the winter half of the year, Yamaguchi et al. (2012) only assessed the summer interannual variations of chl *a* to help clarify the influence of the Changjiang's discharge during summer. Although both Shi and Wang (2012) and Yamaguchi et al. (2012) have analyzed the spatial and temporal variability of chl *a* in the eastern China seas, the seasonal and inter-annual variations of phytoplankton blooms have never been investigated. Moreover, little is known about long-term changes of phytoplankton blooms in the eastern China seas, though the marine environment of China has deteriorated significantly over recent decades due to the impact of rapid economic development, increased population and the associated consequences of habitat loss, eutrophication, pollution and overfishing (see, for example, Zhang et al., 1999; Jin, 2004; Liu and Diamond, 2005; Dong et al., 2010).

BGD
10, 111–155, 2013

In this study, using abundant in situ dataset from two large cruises (up to 1255 samples), we validate and calibrate the satellite-derive chl *a*. Then, based on 14-yr time series of calibrated SeaWiFS and Aqua/MODIS data, we investigate the seasonal and inter-annual variability and long-term changes of phytoplankton blooms in the eastern China seas. Finally we discuss the possible controlling factors and impacts of the El Niño/Southern Oscillation (ENSO) and Pacific Decadal Oscillation (PDO)

2 Study area and data

2.1 Study area

The study area includes the ECS, YS and BS, with the total area of about 1 million km^2 and an average depth of 63 m from the coastal line to 200 m isobath (Liu et al., 2010a) (Fig. 1a). The BS is an inland shallow sea with average depth of 18 m (Liu et al., 2003a). The YS is located between mainland China and the Korean Peninsula, with its mouth opening to the ECS, the 11th largest marginal sea in the world. The ECS extends from Cheju Island in the north to Taiwan Island in the south, and it is bordered by the Kuroshio Current on the east and the coast of China on the west.

The circulation in the eastern China seas has been extensively investigated (see, for example, Beardsley, 1985; Chao, 1990; Fang et al., 1991; Hu, 1994; Su, 1998; Katoh et al., 2000; Naimie et al., 2001). The strong western ocean boundary current Kuroshio flows northeastward along the ECS shelf at water depths of 200 m to 1000 m. The intrusion of the Kuroshio off northeastern Taiwan combines with the northward flow of the northward Taiwan Warm Current (TWWC) from the Taiwan Strait in summer (Ichikawa and Beardsley, 2002), but from the Kuroshio in winter (Chen and Sheu, 2006). In addition, as the Kuroshio turns eastward toward the Northwestern Pacific, a branching current intrudes onto the shelf and penetrates into the Yellow Sea and even the Bohai Sea, forming the Yellow Sea Warm Current (YSWC, Lie et al., 2001). In summer, the

BGD
10, 111–155, 2013

Changjiang plume (or the Changjiang Diluted Water, CDW) extends northeastward to the shelf, broadly forced by the southwest monsoon (Chang and Isobe, 2003).

2.2 Data

2.2.1 Satellite ocean color data sets

The daily and 8-day composite chl *a* and remote sensing reflectance at 555 nm (*Rrs555*) retrieved by SeaWiFS and Aqua/MODIS were acquired from the NASA ocean color website (http://oceancolor.gsfc.nasa.gov). The spatial resolution of the data sets is 5′ with global coverage. The SeaWiFS dataset spans January 1998 to December 2007, and the Aqua/MODIS dataset spans January 2003 to December 2011. Although SeaWiFS worked successfully until the end of 2010, data is unavailable for several months after 2008 due to technical difficulties with the sensor. To preserve statistical rigor, we discard the SeaWiFS data after 1 January 2008.

The daily chl *a* data sets were used to validate and calibrate the satellite-derive chl *a*. We matched the daily chl *a* from SeaWiFS and Aqua/MODIS with in situ data from the same daily time window. Since the daily satellite-derive chl *a* data suffered by heavy cloud masking, we used the 8-day composite chl *a* data sets to obtain the statistics of phytoplankton blooms. In addition, to illustrate the turbidity of coastal water, we also used the satellite-derive *Rrs555*, which has been demonstrated to be a good indicator of water turbidity with larger *Rrs555* corresponding to high turbidity (Yamaguchi et al., 2012).

2.2.2 In situ data sets of chl *a*

In situ data sets of chl *a* from two large cruises covering all the eastern China seas were collected in this study to validate and calibrate the satellite-derive chl *a* data, as shown in Fig. 1b and c. These cruises were initiated and powerfully organized by the State Oceanic Administration (SOA) of China, and more than five vessels were used

BGD
10, 111–155, 2013

to conduct the investigations synchronously throughout the eastern China seas. The summer cruises were undertaken from 15 July to 31 August 2006, and occupied 662 stations. The winter cruises were from 19 December 2006 to 4 February 2007, and occupied 593 stations. The two cruises had almost the same sampling stations and used the same measurement method for the chl *a*. Water samples for chl *a* were filtered onto 25 mm Whatman GF/F filters with 0.7 µm pore size. The filters were preserved in liquid nitrogen before being processed. Each filter was analyzed fluorometrically to obtain chl *a* in the laboratory. It is a valuable and treasure dataset with a uniform and near-synchronous measurements. In this study, we only used surface layer chl *a* data with measurement depth less than 5 m.

2.2.3 In situ data sets of nutrients

We downloaded the serial oceanographic survey data sets measured along the coast of South Korea from the NOAA National Oceanographic Data Center (NODC). These data sets originate from the Korea Oceanography Data Center (KODC), which date from 1961 to 2005 with most of data collected within 1994–2005. In this study, we use surface layer nitrate and phosphate data sets along three latitudinal sections (35.5130° N, 34.4300° N and 32.0000° N) during 1998–2005 (Fig. 1a), corresponding to the time period of ocean color satellite data sets. The north section has five serial stations named N1 to N5 from west to east, with N1 in the central YS and N5 near the coast (Fig. 1a). The middle section has three serial stations (named M1, M2 and M3 from west to east), and the south section has five serial stations (named S1 to S5 from west to east). At these serial stations, both the nitrate and phosphate concentrations were regularly measured in February, April, June, August, October and December in every year.

In addition, we obtained serial oceanographic survey data sets from Japan Meteorological Agency Web site (http://www.data.kishou.go.jp/kaiyou/db/vessel_obs/data-report/html/ship/ship.php). The surface nitrate and phosphate data sets during 1998–2010 along the famous PN section with six serial stations (named K1 to K6 from west to east) (Fig. 1a) were used in this study. At each serial station, both nitrate and

BGD
10, 111–155, 2013

phosphate concentrations were usually measured at least in January, April, July, and October to represent the four seasons.

3 Identification of phytoplankton blooms by satellite data

3.1 Normalization of satellite chl *a* between SeaWiFS and Aqua/MODIS

Owing to different sensor performances (e.g. bands, calibration accuracy) and retrieval algorithms (e.g. atmospheric correction and chl *a* algorithms), there are inevitable differences between the chl *a* retrieved by SeaWiFS and Aqua/MODIS (Morel et al., 2007). To remove systematic differences, we compared the annual-mean chl *a* derived from the 8-day composite chl *a* data sets from SeaWiFS with that derived from Aqua/MODIS for overlapping periods from 2003 to 2007, as shown in Fig. 2. As will be shown in the next section, both SeaWiFS and Aqua/MODIS overestimate chl *a* at low concentration but SeaWiFS overestimate more. As a result, we normalized SeaWiFS-derive chl *a* by Aqua/MODIS data according to a linear regression on the logarithmic scale based on data in Fig. 2:

$$\log(\mathrm{Chl_N}) = 0.0184 + 1.0760 \times \log(\mathrm{Chl_S}),\ (R = 0.97,\ \mathrm{SD} = 0.13,\ P < 0.0001) \quad (1)$$

where $\mathrm{Chl_S}$ and $\mathrm{Chl_N}$ are the pre- and post-normalized SeaWiFS-derive chl *a*, respectively; R is the correlation coefficient, and SD is the standard deviation.

3.2 Validation and calibration of satellite-derive chl *a*

To validate the accuracy of satellite-derive chl *a*, we matched the daily satellite-derive chl *a* with in-situ data from two cruises (Fig. 1b, c) at the same daily time window. Figure 3a, b shows comparisons of all matched data for SeaWiFS and Aqua/MODIS. It needs to be noted that the SeaWiFS chl *a* in Fig. 3 were normalized by Eq. (1). Owing to heavy cloud coverage for the daily satellite chl *a* data, there are only a total of

BGD
10, 111–155, 2013

116 and 108 effective match-ups for SeaWiFS and Aqua/MODIS, respectively. Generally, both SeaWiFS and Aqua/MODIS have good performance for chl *a* retrieval in the eastern China seas including in highly turbid waters, although satellite data significantly overestimate the chl *a* in turbid waters with $Rrs555 > 0.005\,sr^{-1}$, as revealed by Fig. 3c, d. In addition, we can see that high water turbidity results in the overestimation of the satellite-derive chl *a* for low concentrations (chl $a < 3\,\mu g\,L^{-1}$), but underestimation for high concentrations. Thus, high water turbidity blurs the chl *a* signal for satellite retrieval, and causes lower variation of the satellite-derive chl *a* than in reality.

In the middle and outer shelves with $Rrs555 < 0.005\,sr^{-1}$, satellite-derive chl *a* are consistent with in situ data, as shown in Fig. 3e, f. Although there are systematic overestimations in the satellite-derive chl *a*, both SeaWiFS and Aqua/MODIS can successfully retrieve chl *a* varying from $0.1\,\mu g\,L^{-1}$ to more than $10\,\mu g\,L^{-1}$. To eliminate the systematic overestimations, we calibrated the satellite-derive chl *a* with the linear regressions derived from the data in Fig. 3e, f for SeaWiFS and Aqua/MODIS, as follows:

$$\begin{cases} \log(\mathrm{Chl}_{C(SWF)}) = 0.3350 + 0.6846 \times \log(\mathrm{Chl}_{N(SWF)}), \\ \qquad\qquad (R = 0.80,\ \mathrm{SD} = 0.34,\ P < 0.0001) \\ \log(\mathrm{Chl}_{C(MOD)}) = 0.3093 + 0.7358 \times \log(\mathrm{Chl}_{(MOD)}), \\ \qquad\qquad (R = 0.86,\ \mathrm{SD} = 0.31,\ P < 0.0001) \end{cases}$$

where, Chl_C is the chl *a* after calibration with suffixes SWF and MOD corresponding to SeaWiFS and Aqua/MODIS, respectively; $\mathrm{Chl}_{N(SWF)}$ is the SeaWiFS-derived chl *a* after being normalized with Eq. (1), and $\mathrm{Chl}_{(MOD)}$ is the Aqua/MODIS-derived chl *a*.

3.3 Identification of blooms in marginal sea with turbid waters

To determine the bloom frequency in certain regimes, threshold criteria of chl *a* of blooms should be defined. It is quite difficult to define the threshold criteria to identify phytoplankton blooms in turbid waters because of the significant overestimation of the satellite-derive chl *a*, as revealed by Fig. 3c, d. Figure 4 shows the climatological annual-mean distributions of satellite-derive chl *a* and its standard deviation, and the

BGD
10, 111–155, 2013

annual-mean *Rrs555* derived from all 8-day composite data sets from SeaWiFS (1998–2007) and Aqua/MODIS (2003–2011). The spatial patterns of annual-mean chl *a* are quite similar to *Rrs555*, with gradual decreases from coast to shelf. In addition, it can be clearly seen that annual-mean chl *a* is very high with low temporal variation (small standard deviation) along the turbid coastal waters year-round, which is expected to be caused by the significant overestimation by satellite-derive chl *a* (Yamaguchi et al., 2012; Shi and Wang, 2012).

To investigate how much overestimation of satellite-derive chl *a* can be induced by terrestrial particles and CDOM, we derived the maximum chl *a*, maximum and minimum *Rrs555* from all 8-day composite data sets from SeaWiFS (1998–2007) and Aqua/MODIS (2003–2011), as shown in Fig. 5. In the Hangzhou Bay (HZB), Changjiang river mouth (CJM), Subei shallow (SBS) and Huanghe river mouth (HHM) where waters are extremely turbid, the maximum chl *a* is generally less than $10\,\mu g\,L^{-1}$ for both SeaWiFS and Aqua/MODIS. This indicates that the overestimation of the satellite-derive chl *a* induced by terrestrial particles and CDOM is less than $10\,\mu g\,L^{-1}$. Also, from the validation results shown in Fig. 3a, b, we can see that the chl *a* for highly turbid water with highest *Rrs555* are less than $10\,\mu g\,L^{-1}$, which supports the result derived from the satellite data. Therefore, $10\,\mu g\,L^{-1}$ is a conservative critical threshold for the identification of phytoplankton blooms in marginal sea with turbid waters. In the following, we used $10\,\mu g\,L^{-1}$ as threshold to identify blooms in the eastern China seas.

3.4 Statistical determination of bloom events

We binned the whole study area into $0.25^\circ \times 0.25^\circ$ grid cells. The 8-day composite satellite chl *a* data was projected into grid cells. For a certain time period (e.g. seasonal, annual), the statistical parameters were calculated as follows:

1. The percentage of valid chl *a* in a grid cell:

$$PE = 100\,\% \times \sum_{i=1}^{N} I_{Chl}/N \qquad (2)$$

BGD
10, 111–155, 2013

where N is the total number of the projected 8-day composite satellite chl a data in a certain period, e.g. $N = 46$ in a year for one satellite; and $I_{Chl} = 1$ if there is at least one projected pixel with a valid value (chl $a > 0$) within the cell, otherwise, $I_{Chl} = 0$. For satellite ocean color remote sensing, PE is mostly determined by the cloud coverage, and its value directly reflects the degree of cloud coverage.

2. Bloom occurrence frequency in a grid cell:

$$F_{bloom} = 100\% \times \sum_{i=1}^{N} I_{bloom} / \sum_{i=1}^{N} I_{Chl} \quad (3)$$

where $I_{bloom} = 1$ for a bloom event occurring in a grid cell, otherwise, $I_{bloom} = 0$. A bloom event was said to be occurred in a grid cell if at least one projected pixel within the cell has chl a larger than the threshold.

3. Bloom intensity index in a specific region:

$$BI = \sum_{i=1}^{M} (F_{bloom} \times S_{bloom} \times A)_{cell} \quad (4)$$

where M is the total number of cells in the specific region; S_{bloom} is the averaged chl a of all bloom events that occurred in a cell; and A is the area of a cell. BI is an area-integrated parameter representing the chl a inventory of phytoplankton blooms in surface 1 m layer in a specific region with unit of kg m^{-1}.

4 Results

4.1 Climatological annual distribution of blooms

Ocean color satellite data are strongly affected by cloud coverage, and the credibility of bloom event statistics may be affected by the percentage of valid data (PE). Figure 6a

BGD
10, 111–155, 2013

shows the annual climatology of PE derived by all 8-day composite chl *a* data sets of SeaWiFS (1998–2007) and Aqua/MODIS (2003–2011). Generally, PE is greater than 50 % in all the eastern China seas, except in the extremely high turbid waters of HZB, CJM, SBS, and HHM. In extremely high turbid waters, the failure of the atmospheric correction or saturation of the radiances measured by Aqua/MODIS would result in the invalid satellite-derive chl *a* (He et al., 2012). Among the eastern China seas, the BS and northern Yellow Sea (NYS) have the lowest cloud coverage with PE larger than 75 %. Although the cloud coverage is relatively heavy in the ECS, especially along the Kuroshio and along the inner shelf, the PE is still greater than 50 %. Thus, the statistics of blooms are expected to be reasonable and meaningful.

Figure 6b shows the annual climatology of F_{bloom} derived from all 8-day composite chl *a* data of SeaWiFS (1998–2007) and Aqua/MODIS (2003–2011). Blooms mostly occur in the Changjiang Estuary (CJE) and the coasts of Zhejiang (CZJ), where maximum F_{bloom} is larger than 25 %. Meanwhile, along some stretches of the coasts of the NYS and BS, F_{bloom} is also as high as 25 %, though the area with high F_{bloom} is much smaller than that in the CJE and CZJ. In the middle of the southern Yellow Sea, F_{bloom} is as high as 5 % mainly due to the spring blooms. Compared to the coastal waters, F_{bloom} in the middle and outer shelves of ECS is less than 3 %. In the oligotrophic Kuroshio, there was almost no strong bloom that occurred in this region. In addition, no strong bloom occurred in the extremely turbid waters in the HZB, CJM and SBS, which is further evidence for the suitability of taking 10 $\mu g L^{-1}$ as the threshold for identifying a bloom event in marginal sea with turbid waters.

4.2 Climatological seasonal distribution of blooms

Figure 7 shows the seasonal climatologies of F_{bloom} and PE derived from all the 8-day composite chl *a* data of SeaWiFS (1998–2007) and Aqua/MODIS (2003–2011). The spring, summer, autumn and winter are defined as April to June, July to September, October to December, and January to March, respectively. Both F_{bloom} and PE have significant seasonal variations, with most of the blooms occurring in spring and

BGD
10, 111–155, 2013

summer. In spring, the highest F_{bloom} occurs along the CJE and CZJ. Along some parts of the BS and NYS, there are also large F_{bloom} values in spring. In addition, spring phytoplankton blooms occur in the central YS with F_{bloom} values up to 8 %. In summer, the region with high F_{bloom} along the CZJ shrinks to the northern part. Meanwhile, the high F_{bloom} in the CJE extends northeastward along the CDW during summer. The spring blooms occurring in the central YS disappear in summer. Similar to the CJE, the west coasts of the Korea peninsula also have high F_{bloom} values. F_{bloom} reaches its highest in summer in the BS. In autumn, F_{bloom} is much smaller as compared to spring and summer, and the high F_{bloom} values are located at the NYS, CJE, and CZJ. In addition, autumn blooms are found in the central YS. In winter, the bloom frequencies decrease further compared to those in the autumn, with high F_{bloom} values still occurring at the NYS. In addition, in the middle shelf of the southern ECS, short-term blooms occur in winter.

Regarding the seasonal variations of PE (Fig. 7), summer has the highest value, indicating the minimal cloud coverage year-round in the eastern China seas. The spatial distribution of PE is quite uniform, with PE larger than 75 % in summer, except in the extremely turbid waters in the HZB, CJM, and SBS. Winter has the lowest PE, with values of less than 50 % in the ECS and a minimum less than 25 %. The low PE may affect the statistics in winter, but with the combination of the 14 yr and two satellite data sets, the impact of low PE may not be significant as evidenced by the poor correlation of the spatial distributions of F_{bloom} and PE in winter.

4.3 Inter-annual variation during the past 14 yr

Figure 8 presents the annual PE derived from SeaWiFS and Aqua/MODIS during the past 14 yr. The spatial distributions of annual PE for all years from both two satellites data are quite similar with high values in the BS and YS, and low values in the ECS. The averaged annual PE for the whole eastern China Seas derived from SeaWiFS and Aqua/MODIS are very consistent with each other in both quantity and inter-annual variation (Fig. 9). Both SeaWiFS and Aqua/MODIS show that the annual PE averaged

BGD
10, 111–155, 2013

over all the whole eastern China seas fluctuates from 55 % to 65 % during the past 14 yr, with the minimum value in 2006. In addition, there are slightly long-term decreasing trends for both the annual PE values derived from SeaWiFS and Aqua/MODIS.

Figure 10 presents the annual F_{bloom} derived from SeaWiFS and Aqua/MODIS during the past 14 yr. Similar to the annual climatology, high F_{bloom} occurs in the CJE and CZJ, but with significant inter-annual variation. To quantitatively examine the inter-annual variation of F_{bloom}, we selected two regions with a high frequency of bloom occurrence in the eastern China seas to obtain the annual bloom intensity index (BI) defined by Eq. (3), as shown in Fig. 11a. Region A located at the CJE corresponds to the area strongly influenced by Changjiang runoff. Region B covers the BS and YS, corresponding to the area weakly influenced by the Changjiang plume. These two regions cover almost all the areas with high F_{bloom}. Figure 11b, c shows the annual BI derived by SeaWiFS and Aqua/MODIS during 1998 to 2011 in these two regions. Although there are systematic differences of the annual BI derived by SeaWiFS and Aqua/MODIS, the inter-annual variations are quite consistent. Region A in the CJE has significant inter-annual variation, but it has no significant increasing or decreasing trends over the long term, as revealed by Fig. 11b. However, in region B covering the YS and BS, there is a significant long-term increase after 2002 and the BI increases by more than two times during the past 14 yr (Fig. 11c).

5 Discussion

The necessary prerequisites for the start of a phytoplankton bloom are the availability of inorganic nutrients and sufficient solar radiation (Fennel et al., 1999). From the seasonal climatology of bloom occurrence frequency as revealed by Fig. 7, we can see that phytoplankton blooms mainly occur in spring and summer. Indeed, the ECS and YS feature spring phytoplankton blooms, while the highest ocean primary production occurs in late summer and early autumn in the BS (Gong et al., 2003; Shi and Wang, 2012). Since the eastern China seas are located in the middle latitudes, available light

BGD
10, 111–155, 2013

is not a limiting factor for phytoplankton blooms in spring and summer, except in highly turbid coastal waters. Therefore, nutrient supply is expected to be the major factor controlling the inter-annual variation of phytoplankton blooms in the eastern China seas. Thus, in the following sections, we focus on the discussion of the nutrient supply in the two typical areas of Region A and Region B in Fig. 11a.

5.1 Impacts of the Changjiang discharge

The Changjiang is the world's fifth largest river in terms of volume discharge, and the fourth largest in terms of sediment load (Milliman and Farnsworth, 2011). The huge discharge of the Changjiang exports abundant terrestrial materials to the estuary and further to large plume areas. On one hand, the Changjiang inputs large amounts of nutrients into the CJE, benefiting phytoplankton blooms. The annual nutrient flux to the CJE from the Changjiang is markedly higher than that from other estuaries in China (Shen et al., 1992). The annual fluxes of total inorganic nitrogen, phosphate, silicate and nitrate are about 8.9×10^6 t, 1.4×10^4 t, 2.0×10^6 t and 6.4×10^6 t, respectively, which are an order of magnitude higher than the inputs from the Huanghe (Gao and Song, 2005). On the other hand, the annual sediment load of the Changjiang is about 4.9×10^8 t with an average suspended sediment concentration of about 500 mg L^{-1} (Gao and Song, 2005). As a result, phytoplankton growth was light limited in the water column; phytoplankton therefore grew slowly relative to dilution and vertical mixing and could not accumulate in the euphotic zone in the estuary in spite of high nutrient concentrations (Yin et al., 2004; Wang et al., 2010). Thus, phytoplankton blooms mostly occur in the plume area outside the turbidity maximum in regions rich with terrestrial nutrients and low water turbidity (Fig. 8) (Zhu et al., 2009). The strong phytoplankton blooms combined with column stratification and inflow of bottom water of the TWS lead to the development of hypoxia off the CJE during summer time (Wang et al., 2012).

Since the Changjiang is a major source of nutrients supplying for the inshore area of the ECS (Zhang, 1996; Chai et al., 2009), inter-annual variation of the Changjiang discharge may control bloom intensity in the CJE (Chen et al., 2007). Figure 12a shows

BGD
10, 111–155, 2013

the monthly mean discharges of the Changjiang from 1998 to 2011. The discharges were measured at the Datong Gauge Station, which has no tidal influence, and is 624 km upstream from the river mouth. The maximum discharge occurs mostly in June or July, inducing the highest bloom frequency during summer in the CJE as revealed by Fig. 7. Over the past 14 yr, years 1998 and 2010 had the largest discharges, while years 2006 and 2011 had the lowest discharges. The maximum monthly discharges for 1998 and 2010 are 63 426 and 61 310 $m^3 s^{-1}$, while they are 38 534.48 and 36 916.13 $m^3 s^{-1}$ for 2006 and 2011, respectively.

Generally, annual BI covaries with annual mean discharge as revealed by Fig. 12b, indicating that the Changjiang discharge is related to blooms in the CJE. Using 10 yr (1998 to 2006) of SeaWiFS-derive chl *a* data, Yamaguchi et al. (2012) also found that summer chl *a* maxima between 1998 and 2006 in the CJE were positively correlated with Changjiang discharge with a time lag of 0–2 months, suggesting that interannual variation of chl *a* was controlled by interannual variation of Changjiang discharge. Yet, from Fig. 12b, we can see that there are anomalies in several years, especially in 2006, suggesting that other factors might additionally affect the phytoplankton blooms besides river discharge, such as the direction and area of the plume extension, the stability of the water column, tidal cycles, wind forcing, and grazing rates of zooplankton (Cloern, 1996; Yin et al., 2004). At the same time, increases of both nitrogen and phosphorus and decreases in silicate from the outflow of the Changjiang may have disrupted the ecosystem in the ECS, although the exact effect is yet unknown (Zhou et al., 2008; Zhu et al., 2009). In addition, the construction of the Three Gorges Dam (TGD), the world's largest hydropower project, impounded from June 2003, has reduced the sediment load to 147 Mt yr^{-1} in 2004, which is 35 % of the average for the previous five decades (Yang et al., 2006; Xu and Milliman, 2009).

Comparing with the SeaWiFS-derived monthly Changjiang plumes in July–August during 1998 to 2010 (Bai et al., 2013b, or see Fig. 16) which were inversed by the SeaWiFS-retrieved absorption coefficient of colored dissolved organic matter (CDOM) (Bai et al., 2013a), the BI distributions are consistent well with the plume areas with

BGD
10, 111–155, 2013

salinity < 28. Large bloom areas correspond to large plumes. The maximum blooms occur in 1998 and 2003 with largest plume area for SeaWiFS during 1998–2007, and minimum blooms in 2001 and 2004 with smallest plume areas. In 1999, the blooms move to southward because of the southward extending of Changjiang plume. Similarly, the maximum blooms occur in 2003 and 2010 with largest plume area for Aqua/MODIS during 2003–2011, and minimum blooms in 2004 and 2008 with smallest plume areas. It needs to be noted that the plume areas in 2006 is not small in spite of the minimum discharge among the 1998–2010, which may explain the anomaly of the mismatch between BI and Changjiang discharge in 2006 as shown in Fig. 12b.

Regarding long-term changes of BI as shown in Fig. 11b, we can see that there is no significant long-term increase or decrease during the past 14 yr in the CJE in despite of the significant inter-annual variation. Despite the large reduction of sediment after the construction of the TGD, water discharge has had no corresponding significant decrease (Chai et al., 2009; Xu and Milliman, 2009). Therefore, the impacts of the TGD on annual discharge and associated nutrients are expected to be limited, as evidenced by the annual mean discharge in Fig. 12b. In addition, the significant decrease of suspended sediment supply by the Changjiang could increase water transparency in the estuary and favor phytoplankton blooms, which can compensate for the effect of nutrient reduction due to the slight decrease of river discharge. It needs to be noted that the general trend derived in this study is for 1998–2011. Studies have revealed that nutrients added by the Changjiang have increased dramatically since the 1960s, mainly due to the use of chemical fertilizers and industrial/domestic sewage discharges (Zhang, 1996; Gao and Wang, 2008; Zhou et al., 2008).

5.2 Doubling of bloom intensity in the YS and BS

Both SeaWiFS and Aqua/MODIS reveal a doubling of the bloom intensity during the past 14 yr in the YS and BS (Fig. 11c). The doubling of blooms is very significant and important for biogeochemical processes and the marine carbon cycle because of the high background biomass in these regions (Fig. 4a, d). Using 10 yr (September

BGD
10, 111–155, 2013

1997 to October 2006) of monthly-mean chl *a* data observed by SeaWiFS, Yamaguchi et al. (2012) also found that the chl *a* during summer gradually increased over 10 yr in the YS, indicating possible eutrophication. Therefore, a natural question to ask is whether nutrients have significantly increased in these regions or not?

Figure 13 shows the temporal variations of surface layer nitrate and phosphate concentrations along two latitudinal sections in the southeastern YS (Fig. 1a) during 1998–2005. The maximum concentrations of nitrate and phosphate generally occur in December or February due to strong vertical mixing in the winter. As expected, both the nitrate and phosphate concentrations along the two sections increase significantly from 1998 to 2005. At the central YS represented by station N1, the maximum nitrate concentration increases from 6.84 $\mu mol\,L^{-1}$ in 1998 to 14.61 $\mu mol\,L^{-1}$ in 2005. The maximum phosphate concentration increases from 0.41 $\mu mol\,L^{-1}$ in 1998 to 1.01 $\mu mol\,L^{-1}$ in 2005. Similarly, at station M1 located in the central YS, the maximum nitrate concentration increases from 5.58 $\mu mol\,L^{-1}$ in 1998 to 11.17 $\mu mol\,L^{-1}$ in 2005, and from 0.58 $\mu mol\,L^{-1}$ in 1998 to 1.13 $\mu mol\,L^{-1}$ in 2005 for the maximum phosphate concentration. The averaged rates of increase for all these serial stations are 0.37 $\mu mol\,L^{-1}$ and 0.05 $\mu mol\,L^{-1}$ per-year for the nitrate and phosphate concentrations, respectively. Therefore, the more than twofold increase of nutrients is expected to support the doubling of the bloom intensity in the YS and BS during the past 14 yr.

Many factors could cause the nutrient increase, such as the incursion of the Kuroshio, and riverine inputs. From the nutrient data along two sections in the Kuroshio and ECS shelf (Fig. 14), we can see that there are no significant increases or decrease of nitrate and phosphate concentrations at surface layer during the past 14 yr, indicating that the incursion of Kuroshio might not be the major responsible for the twofold increase of nutrients in the YS. The YS and BS can be described as a river-dominated region with restricted connection to the open ocean. There are nearly 50 rivers carrying large quantities of freshwater discharges, suspended solids, and dissolved nutrients into these seas from western and eastern sides, including the Huanghe, the second largest river in China after Changjiang. The riverine nutrients in the eastern China seas

BGD
10, 111–155, 2013

have increased dramatically during the past decades mainly due to the use of chemical fertilizers and industrial/domestic sewage discharges (Zhang, 1996; Gao and Wang, 2008; Zhou et al., 2008; Qu and Kroeze, 2010). Moreover, water flush time in the YS and BS is about 2.2 yr due to the semi-enclosed boundary, which is much longer than that in the ECS (Liu et al., 2003b). The dramatically increased riverine nutrients and long resident time might be responsible for the systematical increase of nutrients in the YS and BS during the past 14yr. In addition, climate change and dust deposition can additionally impact the nutrients. Using satellite wind data, Chen et al. (2012) found that annual wind speeds increased slightly during 2000–2011 in all the eastern China seas. The increase of wind speed might enhance the vertical mixing and favour the transportation of nutrient-rich bottom water to the euphotic layer. The annual dust input to the entire ECS is estimated to be 17 Mt, which appears to be a significant source of sediments and dissolved Fe compared with riverine discharge (Hsu et al., 2009). Tan et al. (2011) also found that chl *a* and primary production increased and eventually became a bloom 1–21 days after the occurrence of dust storms in the southern YS. It is worthy to investigate the long term trends of dust input while the data is available in the future.

5.3 Relation to the climate change

To examine the impacts of the ENSO and PDO on the blooms in the eastern China seas, we compared the inter-annual variations of the bloom intensity index with the Multivariate ENSO Index (MEI) and PDO index, as shown in Fig. 15. In the Region A in the CJE, the inter-annual variations of bloom intensity index and MEI/PDO match relatively well with high bloom intensity indexes generally occur in warm phases, while low bloom intensity indexes occur in cool phases, as revealed by Fig. 15a, c, indicating that the ENSO and PDO can modulate the bloom intensity in the CJE. The annual mean discharge of Changjiang covaries very well with the ENSO and PDO indexes, as revealed by Fig. 15a, c. This is consistent with the notion that large Changjiang discharges generally occur in warm phases, while low discharges occur in cool phases

BGD
10, 111–155, 2013

(Jiang et al., 2006; Zhang et al., 2007). Therefore, it is expected that because the ENSO and PDO can modulate the Changjiang discharge, the bloom intensity is hence affected in the CJE.

The impacts of the ENSO and PDO on the blooms in the Region B cover the YS and BS are less significant as compared with that in the CJE, as revealed by Fig. 15b, d. Although the twofold increase of nutrients might dominate the doubling of bloom intensity in long term in the YS and BS, the ENSO and PDO can also modulate the inter-annual variation of bloom intensity in this region with increase of bloom intensity occurring in warm phases and decrease of bloom intensity in cool phases. It needs to be noted that our analysis in this study about the relationship between bloom intensity and ENSO or PDO is qualitative and preliminary, and it needs more investigation in the future.

5.4 Uncertainties of statistical results

Up to now, there has been no uniform method and threshold to define phytoplankton blooms. For example, Henson and Thomas (2007) and Siegel et al. (2002) use a value 5 % above the annual median values of surface chl *a* to define the initiation times of blooms. Kim et al. (2009) use two different approaches to define phytoplankton blooms: one is a constant threshold, defined as two standard deviations above the long-term average, and the other is a varying threshold, depending on each year's median value. The constant threshold approach is useful for understanding the long-term changes in phytoplankton blooms, while the varying threshold approach is aimed at understanding the timing and intensity of blooms on annual timescales. In this study, considering the overestimation by satellite data in turbid waters, we use $10\,\mu g\,L^{-1}$ as the threshold to identify blooms over the entire 14 yr. This threshold is within the threshold values of major blooms ($17.9\,\mu g\,L^{-1}$) and minor blooms ($5.7\,\mu g\,L^{-1}$) used by Kim et al. (2009).

The greatest challenge for the analysis of inter-annual variability using satellite ocean color data is the gaps in valid data induced by cloud coverage. Merging multiple satellite datasets may reduce the effect of cloud coverage. However, for long-duration clouds,

BGD
10, 111–155, 2013

improvement from multiple satellites data merging is limited. In the eastern China seas, cloud coverage is quite low in the BS and YS, while it is much greater in the ECS, especially in the winter. The low proportion of valid data makes it difficult to determine phenology statistics of phytoplankton blooms (e.g. initiation date and duration) in the ECS. In this study, to increase the proportion of valid data, we used 8-day composite chl *a* data instead of daily data. The annual mean PE is generally larger than 50 % (Fig. 8), which makes the annual bloom statistics meaningful. In addition, the very low PE in winter in the ECS (less than 25 % in the shelf) makes it difficult to calculate seasonal bloom statistics for each year. Therefore, in this study, we limit the bloom statistics only to the annual scale. Although using the 8-day composite satellite chl *a* data may increase the proportion of valid data compared with daily data, it cannot resolve short-term bloom events with durations shorter than 8 days. In addition, if a bloom event occurs during the one day that is captured by the satellite observation, we assume that this bloom event lasted for 8 days. Therefore, the 8-day temporal resolution may systematically overestimate the bloom occurrence frequency. However, this systematic overestimation is expected to be limited for the annual or climatological statistics in this study.

Another limitation of the statistical results is the difference between SeaWiFS and Aqua/MODIS data. Although we have normalized and calibrated the satellite-derive chl *a* data by in situ measurements, the bloom occurrence frequency derived from SeaWiFS is still systematically lower than that derived from Aqua/MOIDS in the YS and BS, as revealed by Fig. 10. The difference may be caused by multiple factors, including the different sensor bands, atmospheric correction, and chl *a* retrieval algorithms etc., and further efforts should be taken to eliminate this difference in the future.

6 Conclusions

Thanks to the time series of satellite ocean color data provided by SeaWiFS and Aqua/MODIS, the inter-annual variability of phytoplankton blooms could be studied

BGD
10, 111–155, 2013

over the past 14 yr from 1998 to 2011. This study firstly deals with the bloom identification in the turbid water to ensure a proper data set to figure out the bloom variation. Then, this study presented the annual and seasonal climatological distributions of phytoplankton blooms in the eastern China seas and analyzed their spatial and temporal variations. More importantly, this study revealed the doubling of the bloom intensity index in the YS and BS during the past 14 yr, while surprisingly there was no long-term increase or decrease of bloom intensity in despite of significant inter-annual variation in the CJE. The more than twofold increases of nitrate and phosphate concentrations are expected to be responsible for the doubling of the bloom intensity index in the YS and BS.

The present study has also revealed that high water turbidity blurred the chl *a* signal for satellite retrieval, overestimating chl *a* for chl *a* less than $3\,\mu g\,L^{-1}$ and underestimating chl *a* for high chl *a* by satellite. From the 14-yr chl *a* data sets from SeaWiFS and Aqua/MODIS, we found that the overestimation of satellite-derive chl *a* caused by high water turbidity was less than $10\,\mu g\,L^{-1}$, which could be used as a safe threshold for the identification of a phytoplankton bloom in a marginal sea with turbid waters.

This study identified some scientific problems that remain to be solved. The exact sources of the twofold nutrient increase in the YS are still unknown. Moreover, doubling of nutrients and blooms are expected to affect the biomass, primary production, and carbon budget. In addition, more efforts should be taken to improve the satellite retrieval of chl *a* in the eastern China seas, especially to reduce the difference between SeaWiFS and Aqua/MODIS.

Acknowledgements. We thank the SOA of China for providing the in situ chl *a* data sets, and all the crews for their field sampling. We also thank NASA for providing the satellite-derive chl *a* data sets, and NODC, KODC and JMA for providing the in situ nutrients data sets. Financial support has been provided by the National Basic Research Program ("973" Program) of China (grant #2009CB421202), the Public Science and Technology Research Funds Projects of Ocean (grant #200905012), the "908" project of China (grant #908-ZC-I-04, #908-01-ST10), the National Natural Science Foundation of China (grants #41271378, #40976110 and #41271417) and the "Global Change and Air-Sea Interaction" project of China.

BGD
10, 111–155, 2013

References

Bai, Y., Pan, D., Cai, W.-J., He, X., Wang, D., Tao, B., and Zhu, Q.: Remote sensing of salinity from satellite-derived CDOM in the Changjiang River-dominated East China Sea, J. Geophy. Res., doi:10.1029/2012JC008467, in press, 2013a.

Bai, Y., He, X. Q., Pan, D. L., Chen, C. T. A., Kang, Y., Chen, X. Y., and Hao, Z. Z.: Synthetic view of Changjiang River plume variation in summer from 1998–2010, Biogeosciences, in preperation, 2013b.

Beardsley, R. C., Limeburner, R., Yu, H., and Cannon, G. A.: Discharge of the Changjiang (Yangtze River) into the East China Sea, Cont. Shelf Res., 4, 57–76, 1985.

Chai, C., Yu, Z. M., Shen, Z. L., Song, X. X., Cao, X. H., and Yao, Y.: Nutrient characteristics in the Yangtze River Estuary and the adjacent East China Sea before and after impoundment of the Three Gorges Dam, Sci. Total Environ., 407, 4687–4695, 2009.

Chang, P. H. and Isobe, A.: A numerical study on the Changjiang diluted water in the Yellow and East China Seas, J. Geophy. Res., 108, 3299, doi:10.1029/2002JC001749, 2003.

Chao, S.: Circulation of the East China Sea, a numerical study, J. Oceanogr. Soc. Japan, 46, 273–295, 1990.

Chen, C. C., Gong, G. C., and Shiah, F. K.: Hypoxia in the East China Sea: one of the largest coastal low-oxygen areas in the world, Mar. Environ. Res., 64, 399–408, 2007.

Chen, C. T. A.: The Kuroshio intermediate water is the major source of nutrients on the East China Sea continental shelf, Oceanol. Acta, 19, 523–527, 1996.

Chen, C. T. A. and Sheu, D. D.: Does the Taiwan Warm Current originate in the Taiwan Strait in wintertime?, J. Geophy. Res., 111, C04005, doi:10.1029/2005JC003281, 2006.

Chen, C. T. A. and Wang, S. L.: Carbon, alkalinity and nutrient budgets on the East China Sea. J. Geophy. Res., 104, 20675–20686, doi:10.1029/1999JC900055, 1999.

Chen, C. T. A., Ruo, R., Pai, S. C., Liu, C. T., and Wong, G. T. F.: Exchange of water masses between the East China Sea and the Kuroshio off northeastern Taiwan, Cont. Shelf Res., 15, 19–39, 1995.

Chen, X. Y., Pan, D. L., He, X. Q., Bai, Y., Wang, Y. F., and Zhu, Q. K.: Seasonal and interannual variability of sea surface wind over the China seas and its adjacent ocean from QuikSCAT and ASCAT data during 2000–2011, Proc. of SPIE, 8532, 853214, doi:10.1117/12.974573, 2012.

BGD
10, 111–155, 2013

Chen, Y. L., Chen, H. Y., Lee, W. H., Hung, C. C., Wong, G. T. F., and Kanda, J.: New production in the East China Sea, comparison between well-mixed winter and stratified summer conditions, Cont. Shelf Res., 21, 751–764, 2001.

Chen, Y. L., Chen, H. Y., Gong, G. C., Lin, Y. H., Jan, S., and Takahashi, M.: Phytoplankton production during a summer coastal upwelling in the East China Sea, Cont. Shelf Res., 24, 1321–1338, 2004.

Cloern, J. E.: Phytoplankton bloom dynamics in coastal ecosystems: a review with some general lessons from sustained investigation of San Francisco Bay, California, Rev. Geophys., 34, 127–168, 1996.

Dong, Z. J., Liu, D. Y., and Keesing, J. K.: Jellyfish blooms in China: Dominant species, causes and consequences, Mar. Pollut. Bull., 60, 954–963, 2010.

Fang, G., Zhao, B., and Zhu, Y.: Water volume transport through the Taiwan Strait and the continental shelf of the East China Sea measured with current meters, in: Oceanography of Asian Marginal Seas, edited by: Takano, K., Elsevier, New York, 345–358, 1991.

Fennel, K.: Convection and the timing of phytoplankton spring blooms in the western Baltic Sea, Estuar. Coast. Shelf S., 49, 113–128, 1999.

Furuya, K., Hayashi, M., Yabushita, Y., and Ishikawa, A.: Phytoplankton dynamics in the East China Sea in spring and summer as revealed by HPLC-derived pigment signatures, Deep-Sea Res. Pt. II, 50, 367–387, 2003.

Gao, S. and Wang, Y. P.: Changes in material fluxes from the Changjiang River and their implications on the adjoining continental shelf ecosystem, Cont. Shelf Res., 28, 1490–1500, 2008.

Gao, X. L. and Song, J. M.: Phytoplankton distributions and their relationship with the environment in the Changjiang Estuary, China, Mar. Pollut. Bull., 50, 327–335, 2005.

Gong, G. C., Chen, Y. L., and Liu, K. K.: Summertime hydrography and chlorophyll *a* distribution in the East China Sea in summer: implications of nutrient dynamics, Cont. Shelf Res., 16, 1561–1590, 1996.

Gong, G. C., Shiah, F. K., Liu, K. K., Wen, Y. H., and Liang, M. H.: Spatial and temporal variation of chlorophyll *a*, primary productivity and chemical hydrography in the southern East China Sea, Cont. Shelf Res., 20, 411–436, 2000.

Gong, G. C., Wen, W. H., Wang, B. W., and Liu, G. J.: Seasonal variation of chlorophyll *a* concentration, primary production and environmental conditions in the subtropical East China Sea, Deep-Sea Res. Pt. II, 50, 1219–1236, 2003.

BGD
10, 111–155, 2013

Gong, G. C., Chang, J., Chiang, K. P., Hsiung, T. M., Hung, C. C., Duan, S. W., and Codispoti, L. A.: Reduction of primary production and changing of nutrient ratio in the East China Sea: effect of the Three Gorges Dam?, Geophys. Res. Lett., 33, L07610, doi:10.1029/2006GL025800, 2006.

Hama, T., Shin, K. H., and Handa, N.: Spatial variability in the primary productivity in the East China Sea and its adjacent waters, J. Oceanogr., 53, 41–51 1997

He, X. Q., Bai, Y., Pan, D. L., Tang, J. W., and Wang, D. F.: Atmospheric correction of satellite ocean color imagery using the ultraviolet wavelength for highly turbid waters, Opt. Express, 20, 20754–20770, 2012

Henson, S. A. and Thomas, A. C.: Interannual variability in timing of bloom initiation in the California current system, J. Geophy. Res., 112, C08007, doi:10.1029/2006JC003960, 2007.

Hsu, S. C., Liu, S. C., Arimoto, R., Liu, T. H., Huang, Y. T., Tsai, F. J., Lin, F. J., and Kao, S. J.: Dust deposition to the East China Sea and its biogeochemical implications. J. Geophy. Res., 114, D15304, doi:10.1029/2008JD011223, 2009.

Hu, D.: Some striking features of circulation in Huanghai Sea and East China Sea, in: Oceanology of China Seas, vol. 1, edited by: Zhou, D., Liang, Y.-B., and Tseng, C.-K., Kluwer Academic Publishers, Dordrecht, 27–38, 1994.

Hu, H., Wan, Z., and Yuan, Y.: Simulation of seasonal variation of phytoplankton in the southern Huanghai (Yellow) Sea and analysis on its influential factors, Acta Oceanol. Sin., 26, 74–88, 2004.

Hyun, J. H. and Kim, K. H.: Bacterial abundance and production during the unique spring phytoplankton bloom in the central Yellow Sea, Mar. Ecol.-Prog. Ser., 252, 77–88, 2003

Ichikawa, H. and Beardsley, R. C.: The current system in the Yellow and East China Seas, J. Oceanogr., 58, 77–92, 2002.

Isobe, A. and Matsuno T.: Long-distance nutrient-transport process in the Changjiang river plume on the East China Sea shelf in summer. J. Geophy. Res., 113, C04006, doi:10.1029/2007JC004248, 2008.

Jiang, T., Zhang, Q., Zhu, D. M., and Wu, Y. J.: Yangtze floods and droughts (China) and teleconnections with ENSO activities (1470–2003), Quat. Internat., 144, 29–37, 2006.

Jin, X.: Long-term changes in fish community structure in the Bohai Sea, China, Estuarine, Coast. Shelf Sci., 59, 163–171, 2004.

Katoh, O., Morinaga, K., and Nakagawa, N.: Current distributions in the southern East China Sea in summer, J. Geophy. Res., 105, 8565–8573, 2000.

BGD
10, 111–155, 2013

Kim, H. J., Miller, A. J., McGowan, J., and Carter, M.: Coastal phytoplankton blooms in the Southern California Bight, Prog. Oceanogr., 82, 137–147, 2009.
Kiyomoto, Y., Iseki, K., and Okamura, K.: Ocean color satellite imagery and shipboard measurements of chlorophyll *a* and suspended particulate matter distribution in the East China Sea, J. Oceanogr., 57, 37–45, 2001.
Lie, H. J., Cho, C. H., Lee, J. H., Lee, S., Tang Y. X., and Zou, E. M.: Does the Yellow Sea warm Current really exist as a persistent mean flow?, J. Geophy. Res., 106, 22199–22210, 2001.
Liu, J. G. and Diamond, J.: China's environment in a globalizing world, Nature, 435, 1179–1186, 2005.
Liu, K. K., Atkinson, L., Quiñones, R., and Talaue-McManus, L. (Eds.): Carbon and Nutrient Fluxes in Continental Margins: a Global Synthesis, IGBP Book Series, Springer, Heidelberg, Germany, 744 pp., XXVIII, 2010a.
Liu, K. K., Chao, S. Y., Lee, H. J., Gong, G. C., and Teng, Y. C.: Seasonal variation of primary productivity in the East China Sea: a numerical study based on coupled physical-biogeochemical model, Deep-Sea Res. Pt. II, 57, 1762–1782, 2010b.
Liu, S. M., Zhang, J., and Jiang, W. S.: Pore water nutrient regeneration in shallow coastal Bohai Sea, China, J. Oceanogr., 59, 377–385, 2003a.
Liu, S. M., Zhang, J., Chen, S. Z., Chen, H. T., Hong, G. H., Wei, H., and Wu, Q. M.: Inventory of nutrient compounds in the Yellow Sea, Cont. Shelf Res., 23, 1161–1174, 2003b.
Milliman, J. D. and Farnsworth, K. L.: River Discharge to the Coastal Ocean: a Global Synthesis, Cambridge University Press, Cambridge, UK, 2011.
Morel, A., Huot, Y., Gentili, B., Werdell, P. J., Hooker, S. B., and Franz, B. A.: Examining the consistency of products derived from various ocean color sensors in open ocean (Case 1) waters in perspective of a multi-sensor approach, Remote Sens. Environ., 111, 69–88, 2007.
Naimie, C. E., Blain, C. A., and Lynch, D. R.: Seasonal mean circulation in the Yellow Sea-a model-generated climatology, Cont. Shelf Res., 21, 667–695, 2001.
Ning, X., Liu, Z., Cai, Y., Fang, M., and Chai, F.: Physicobiological oceanographic remote sensing of the East China Sea: satellite and in situ observations J. Geophy. Res. 103, 21623–21636, 1998.
Qu, H. J. and Kroeze, C.: Past and future trends in nutrients export by rivers to the coastal waters of China, Sci. Total Environ., 408, 2075–2086, 2010.

BGD
10, 111–155, 2013

Shi, W. and Wang, M.: Characterization of global ocean turbidity from Moderate Resolution Imaging Spectroradiometer ocean color observations, J. Geophy. Res., 115, C11022, doi:10.1029/2010JC006160, 2010.
Shi, W. and Wang, M.: Satellite views of the Bohai Sea, Yellow Sea, and East China Sea, Prog. Oceanogr., 104, 30–45, 2012.
Shen, Z., Lu, J., Liu, X., and Diao, H.: Distribution characteristics of the nutrients in the Changjiang River estuary and the effect of the Three Gorges Project on it, Stud. Mar. Sin., 39, 109–129, 1992.
Siegel, D. A., Doney, S. C., and Yoder, J. A.: The North Atlantic spring phytoplankton bloom and Sverdrup's critical depth hypothesis, Science, 296, 730–733, 2002.
Son, S. H., Yoo, S. J., and Noh, J. H.: Spring phytoplankton bloom in the fronts of the East China Sea, Ocean Sci. J., 41, 181–189, 2006.
Su, J.: Circulation dynamics of the China Seas north of 18° N coastal segment (12, S), in: The Sea, vol. 11, edited by: Robinson, A. R. and Brink, K. H., Wiley, New York, 483–505, 1998.
Tan, S. C., Shi, G. Y., Shi, J. H., Gao, H. W., and Yao, X. H.: Correlation of Asian dust with chlorophyll and primary productivity in the coastal seas of China during the period from 1998 to 2008, J. Geophy. Res., 116, G02029, doi:10.1029/2010JG001456, 2011.
Tang, D. L., Ni, I. H., Muller-Karger, F. E., and Liu, Z. J.: Analysis of annual and spatial patterns of CZCS-derived pigment concentrations on the continental shelf of China, Cont. Shelf Res., 18, 1493–1515, 1998.
Tang, D. L., Di, B. P., Wei, G. F., Ni, I. H., Oh, I. S., and Wang, S. F.: Spatial, seasonal and species variations of harmful algal blooms in the South Yellow Sea and East China Sea, Hydrobiologia, 568, 245–253, 2006.
Wang, B. D., Wei, Q. S., Chen, J. F., and Xie, L. P.: Annual cycle of hypoxia off the Changjiang (Yangtze River) Estuary, Mar. Environ. Res., 77, 1–5, 2012.
Wang, Y., Shen, J., and He, Q.: A numerical model study of the transport timescale and change of estuarine circulation due to waterway constructions in the Changjiang Estuary, China, J. Mar. Syst., 82, 154–170, 2010.
Xu, K. H. and Milliman, J. D.: Seasonal variations of sediment discharge from the Yangtze River before and after impoundment of the Three Gorges Dam, Geomorphology, 104, 276–283, 2009.

BGD
10, 111–155, 2013

Yamaguchi, H., Kim, H. C., Son, Y. B., Kim, S. W., Okamura, K., Kiyomoto, Y., and Ishizaka, J.: Seasonal and summer interannual variations of SeaWiFS chlorophyll *a* in the Yellow Sea and East China Sea, Prog. Oceanogr., 105, 22–29, 2012.

Yang, S. L., Li, M., Dai, S. B., Liu, Z., Zhang, J., and Ding, P. X.: Drastic decrease in sediment supply from the Yangtze River and its challenge to coastal wetland management, Geophys. Res. Lett., 33, L06408, doi:10.1029/2005GL025507, 2006.

Yin, K. D., Zhang, J. L., Qian, P. Y., Jian, W. J., Huang, L. M., Chen, J. F., and Wu, M. C. S.: Effect of wind events on phytoplankton blooms in the Pearl River estuary during summer, Cont. Shelf Res., 24, 1909–1923, 2004.

Zhang, J.: Nutrient elements in large Chinese estuaries, Cont. Shelf Res., 16, 1023–1045, 1996.

Zhang, J., Zhang, Z. F., Liu, S. M., Wu, Y., Xiong, H., and Chen, H. T.: Human impacts on the large world rivers: would the Changjiang be an illustration?, Global Biogeochem. Cy., 13, 1099–1105, 1999.

Zhang, J., Liu, S. M., Ren, J. L., Wu, Y., and Zhang, G. L.: Nutrient gradients from the eutrophic Changjiang (Yangtze River) estuary to the oligotrophic Kuroshio Waters and re-evaluation of budgets for the East China Sea shelf, Prog. Oceanogr., 74, 449–478, 2007.

Zhang, Q., Yu, C.-Y., Jiang, T., and Wu, Y. J.: Possible influences of ENSO on annual maximum streamflow of the Yangtze River, China, J. Hydrol., 333, 265–274, 2007.

Zhao, Y., Zhao, L., Xiao, T., Zhao, S., Xuan, J., Li, C., and Ning, X.: Spatial and temporal variation of picoplankton distribution in the Yellow Sea, China, Chin. J. Oceanol. Limn., 29, 150–162, 2011.

Zhou, M. J., Shen, Z. L., and Yu, R. C.: Responses of a coastal phytoplankton community to increased nutrient input from the Changjiang (Yangtze) River, Cont. Shelf Res., 28, 1483–1489, 2008.

Zhu, Z. Y., Ng, W. M., Liu, S. M., Zhang, J., Chen, J. C., and Wu, Y.: Estuarine phytoplankton dynamics and shift of limiting factors: A study in the Changjiang (Yangtze River) Estuary and adjacent area, Estuar. Coast. Shelf S., 84, 393–401, 2009.

BGD
10, 111–155, 2013

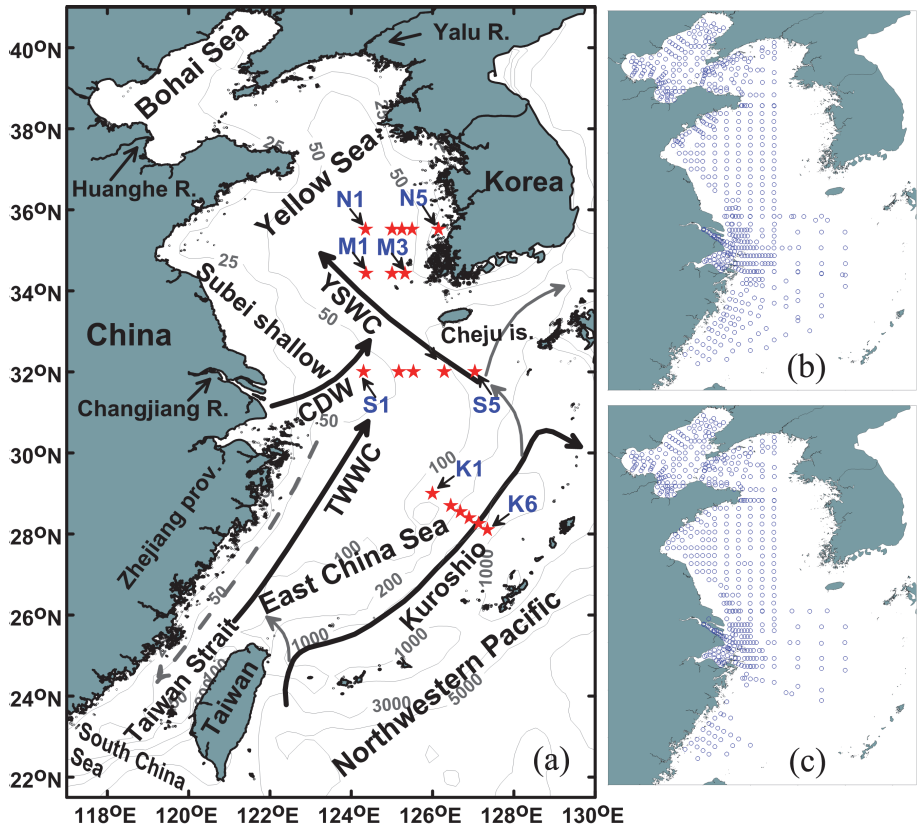

Fig. 1. The bathymetry, schematic circulation, and serial stations along the four sections (N1-N5, M1-M3, S1-S5, K1-K6) in the eastern China seas **(a)**, and the sampling stations of the summer cruises **(b)** and winter cruises **(c)**. TWWC: Taiwan Warm Current, YSWC: Yellow Sea Warm Current, CDW: Changjiang Diluted Water.

BGD
10, 111–155, 2013

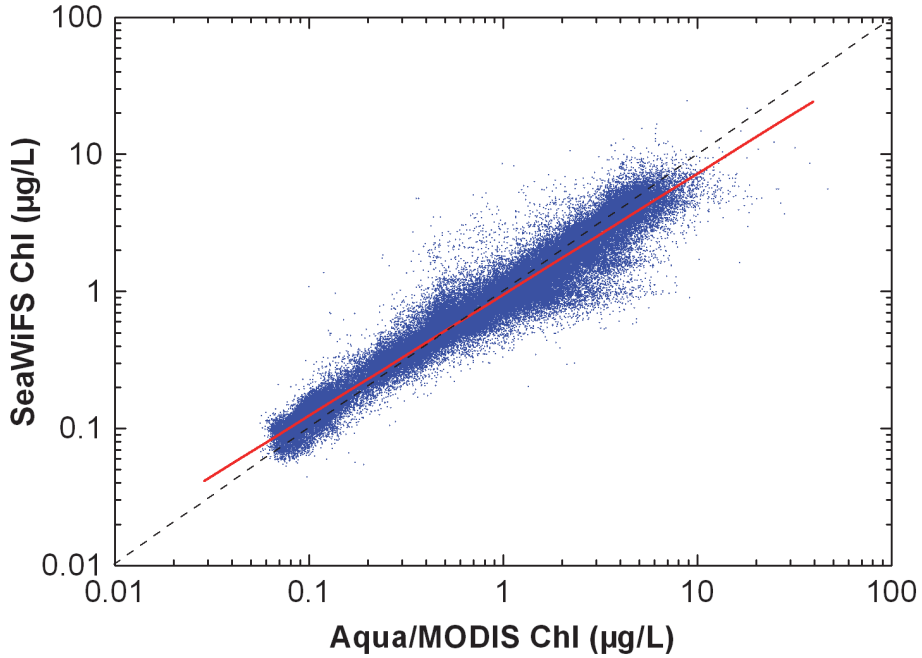

Fig. 2. Comparison of annual-mean chl *a* retrieved by SeaWiFS and Aqua/MODIS during 2003–2007. The black dashed line is the 1 : 1 line, and the red solid line is the linear regression on the logarithmic scale.

BGD
10, 111–155, 2013

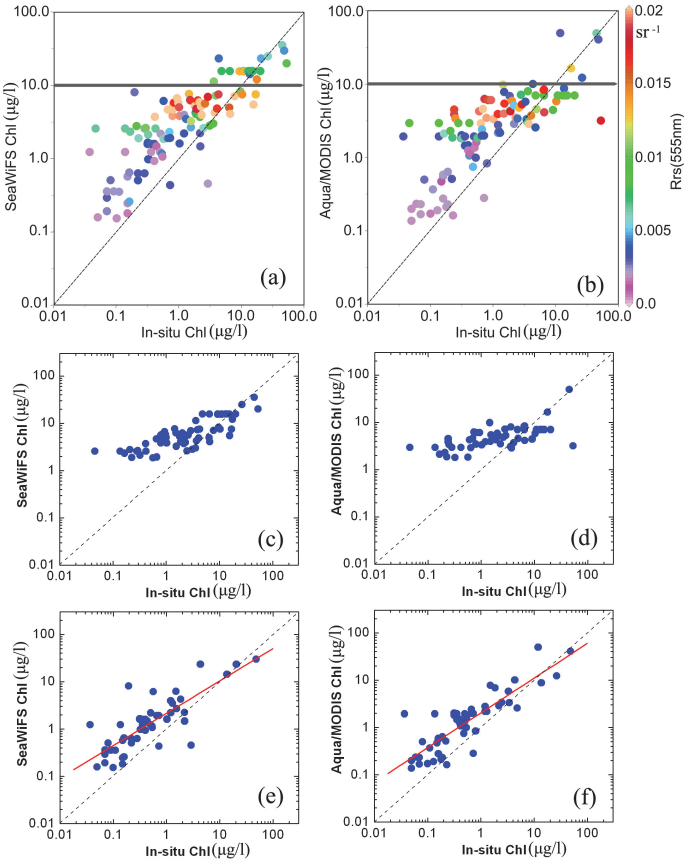

Fig. 3. Comparisons of matched-up chl *a* between daily satellite data and in-situ values according to the same daily time window. The left column is for SeaWiFS, and right column for Aqua/MODIS. **(a)** and **(b)** are for all the matched data; **(c)** and **(d)** are for match-ups with *Rrs555* > 0.005; **(e)** and **(f)** are for match-ups with *Rrs555* < 0.005.

BGD
10, 111–155, 2013

Variability of phytoplankton blooms in the eastern China seas

X. Q. He et al.

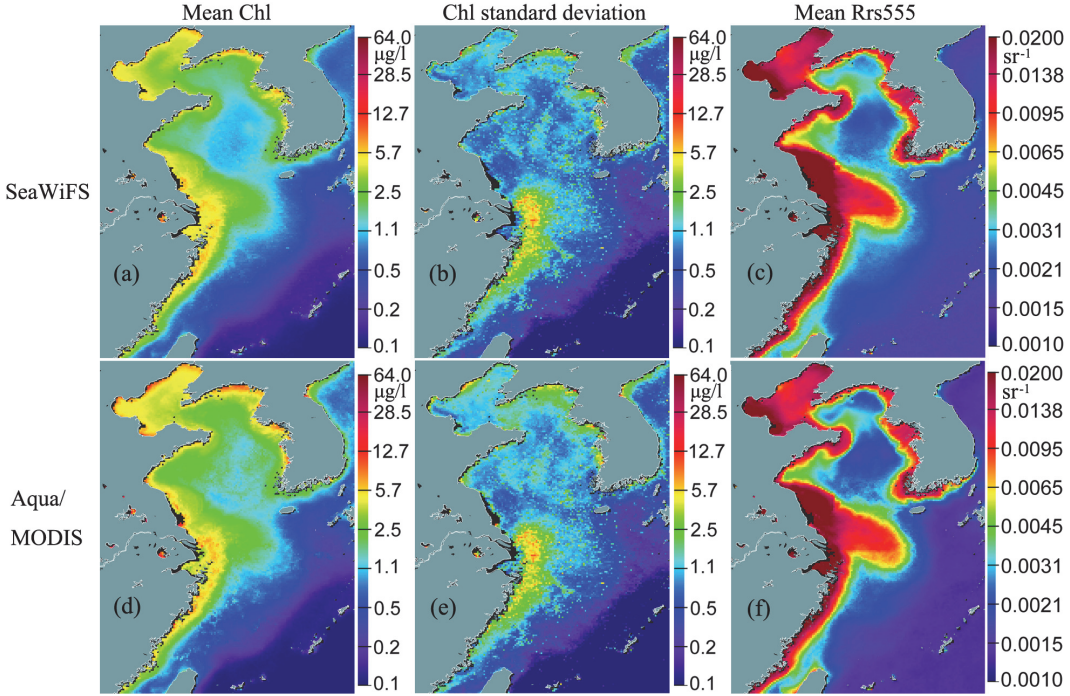

Fig. 4. Climatology distributions of mean (left column) and standard deviation (middle column) of chl *a*, and mean *Rrs555* (right column) retrieved by the SeaWiFS (1998–2007, upper row) and Aqua/MODIS (2003–2011, bottom row).

BGD
10, 111–155, 2013

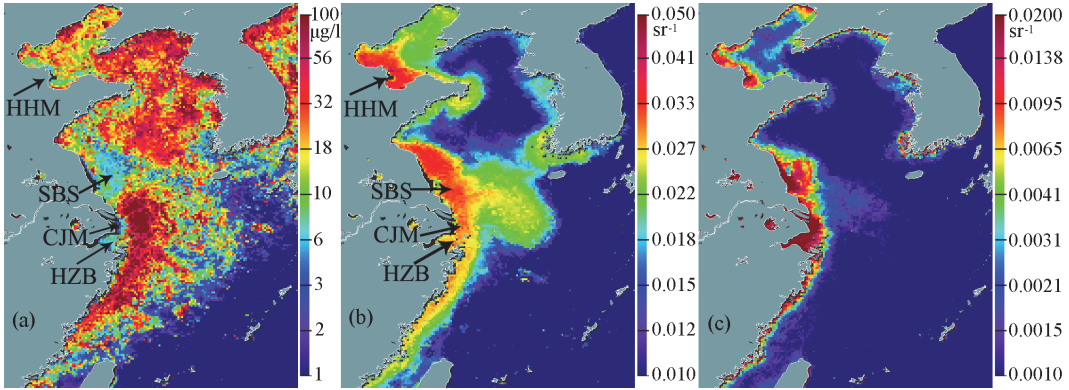

Fig. 5. The spatial distributions of the maximum chl *a* **(a)**, maximum *Rrs555* **(b)** and minimum *Rrs555* **(c)**, retrieved from all 8-day composite chl *a* data sets from SeaWiFS (1998–2007) and Aqua/MODIS (2003–2011). HZB: Hangzhou Bay, CJM: Changjiang river mouth; SBS: Subei shallow; HHM: Huanghe river mouth.

BGD
10, 111–155, 2013

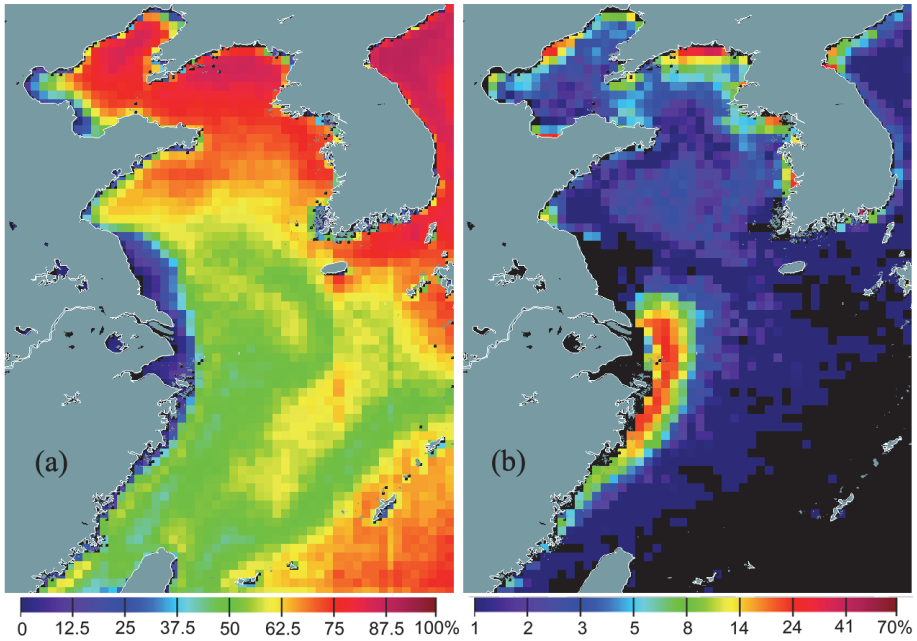

Fig. 6. Annual climatologies of **(a)** PE and **(b)** F_{bloom} derived from all 8-day composite chl *a* data sets from SeaWiFS (1998–2007) and Aqua/MODIS (2003–2011).

BGD
10, 111–155, 2013

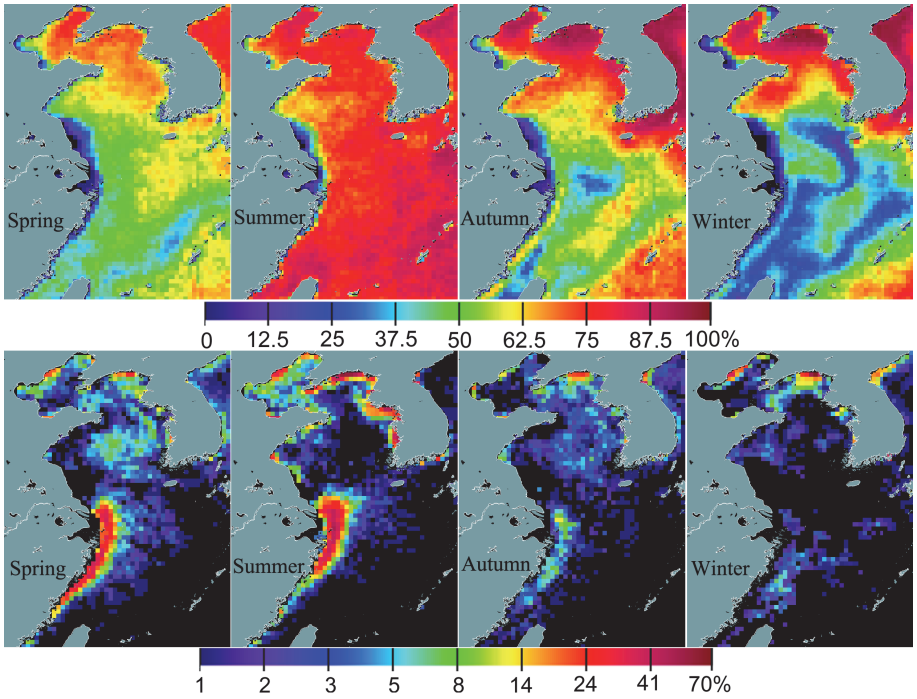

Fig. 7. Seasonal Climatologies of theF_{bloom} (upper row) and PE (bottom row) derived from all 8-day composite chl *a* data from SeaWiFS (1998–2007) and Aqua/MODIS (2003–2011).

BGD
10, 111–155, 2013

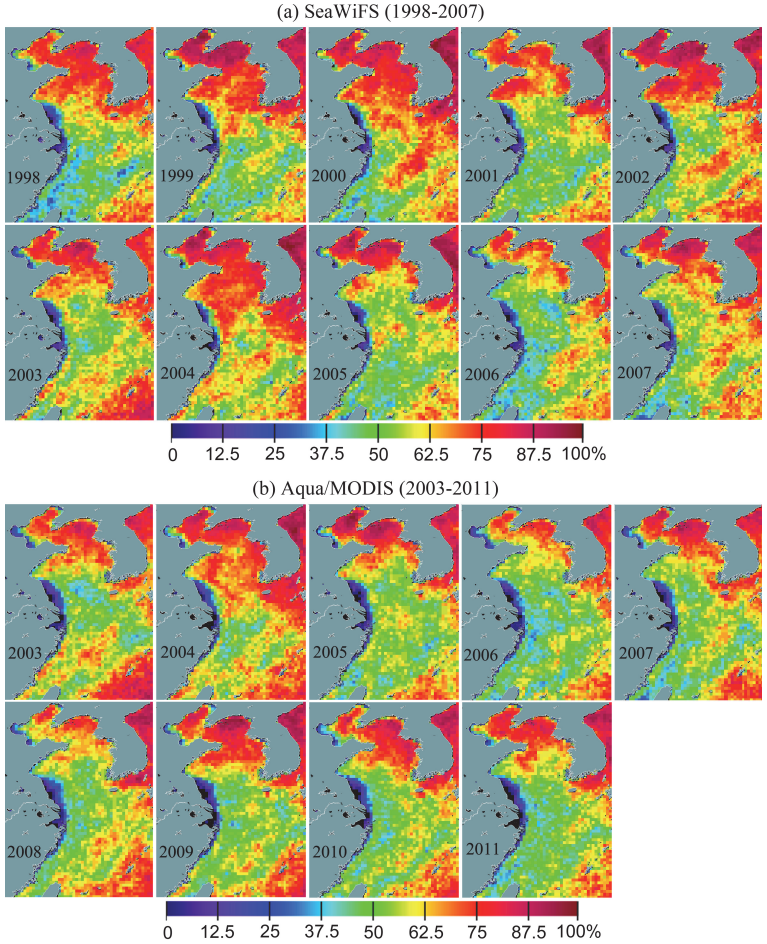

Fig. 8. The annual PE derived from **(a)** SeaWiFS from 1998 to 2007 and **(b)** Aqua/MODIS from 2003 to 2011.

BGD
10, 111–155, 2013

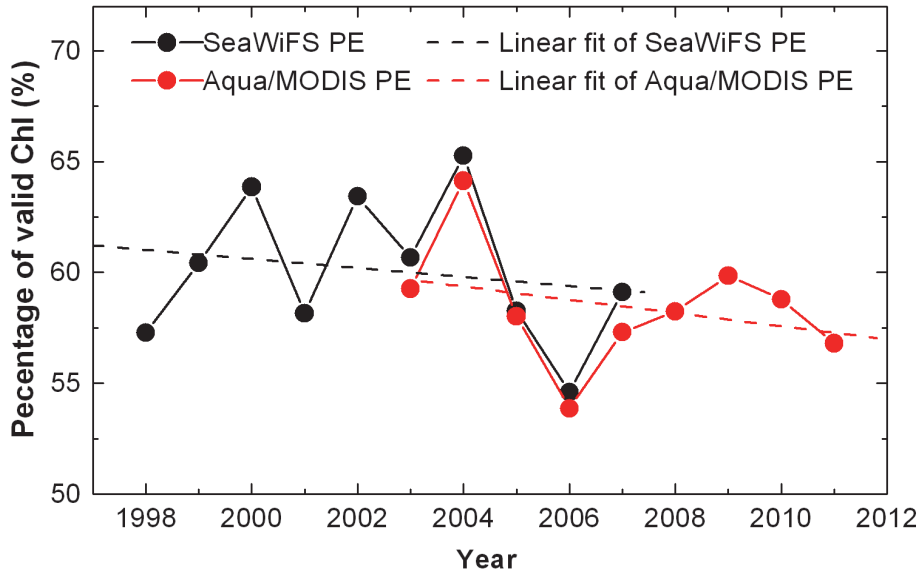

Fig. 9. Inter-annual variation of PE averaged for all the eastern China seas derived from SeaWiFS and Aqua/MODIS.

BGD
10, 111–155, 2013

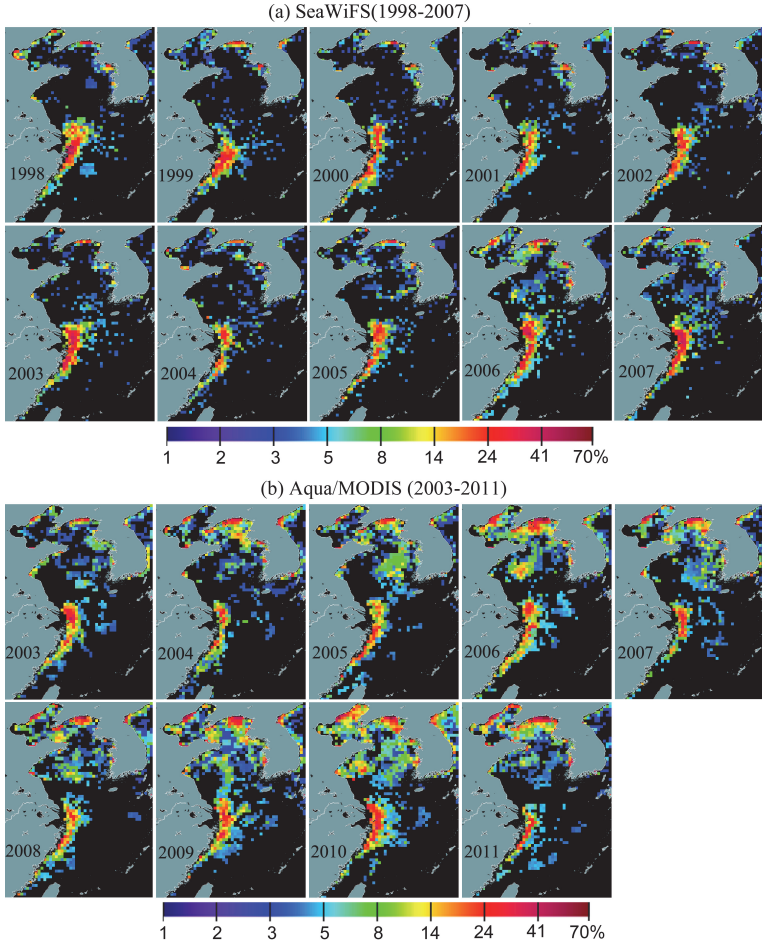

Fig. 10. The annual F_{bloom} derived from **(a)** SeaWiFS from 1998 to 2007 and **(b)** Aqua/MODIS from 2003 to 2011.

BGD
10, 111–155, 2013

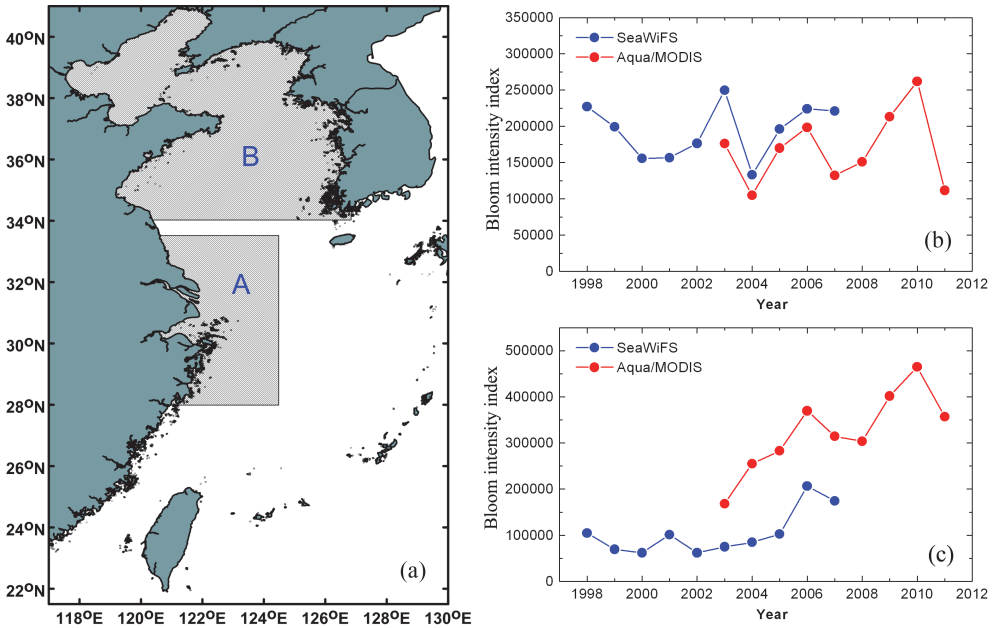

Fig. 11. The locations of the two selected regions in the eastern China Seas **(a)**, and the inter annual variations of the annual bloom intensity index ($kg\,m^{-1}$) in region A **(b)** and region B **(c)** derived from SeaWiFS and Aqua/MODIS.

BGD
10, 111–155, 2013

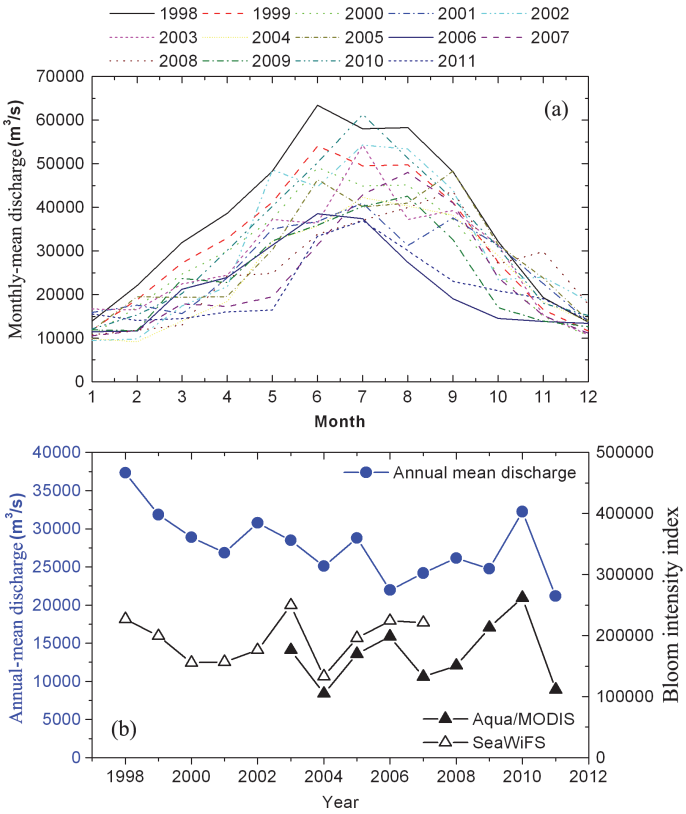

Fig. 12. (a) The monthly averaged Changjiang discharge measured at the Datong Gauge Station during 1998 to 2011 (from http://xxfb.hydroinfo.gov.cn). **(b)** The correlation between the annual bloom intensity index (kg m^{-1}) of region A and annual mean Changjiang discharge during 1998–2011.

BGD
10, 111–155, 2013

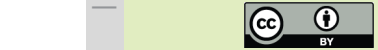

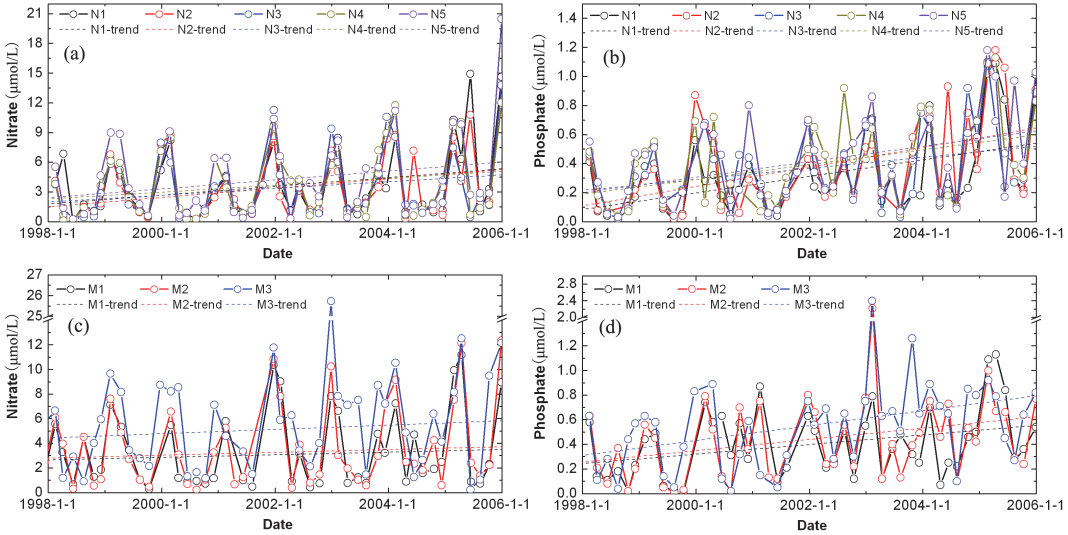

Fig. 13. Temporal variations of nitrate and phosphate concentrations at the serial stations in the southeastern YS during 1998–2005. The upper and lower rows are the sections N1–N5 and M1–M3, respectively, as shown in Fig. 1a. The dash line is the linear regression versus time (year) for each serial station.

BGD
10, 111–155, 2013

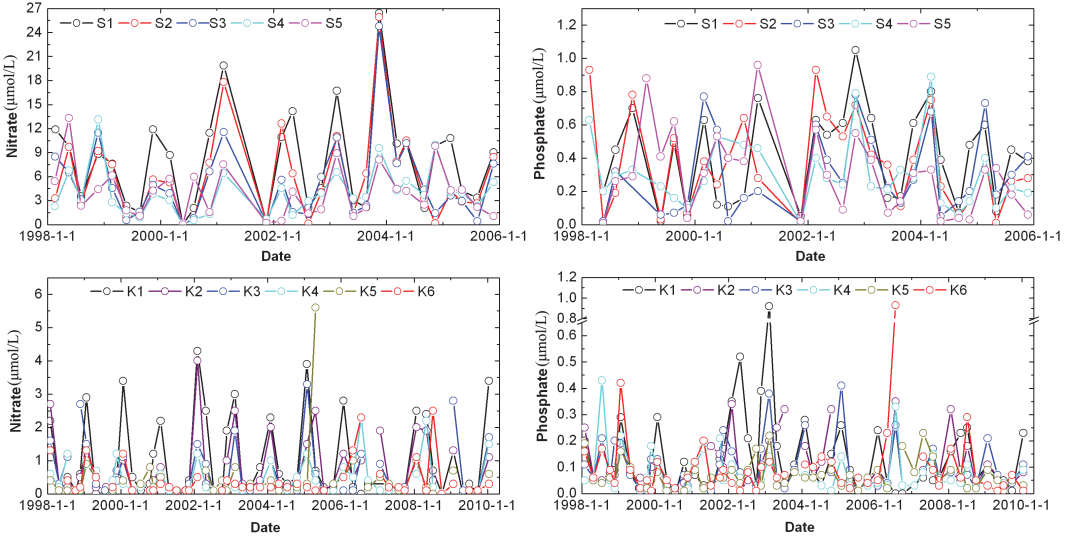

Fig. 14. Temporal variations of nitrate and phosphate concentrations at the serial stations in the ECS during 1998–2005. The upper and lower rows are the sections S1–S5 and K1–K6, respectively, as shown in Fig. 1a.

BGD
10, 111–155, 2013

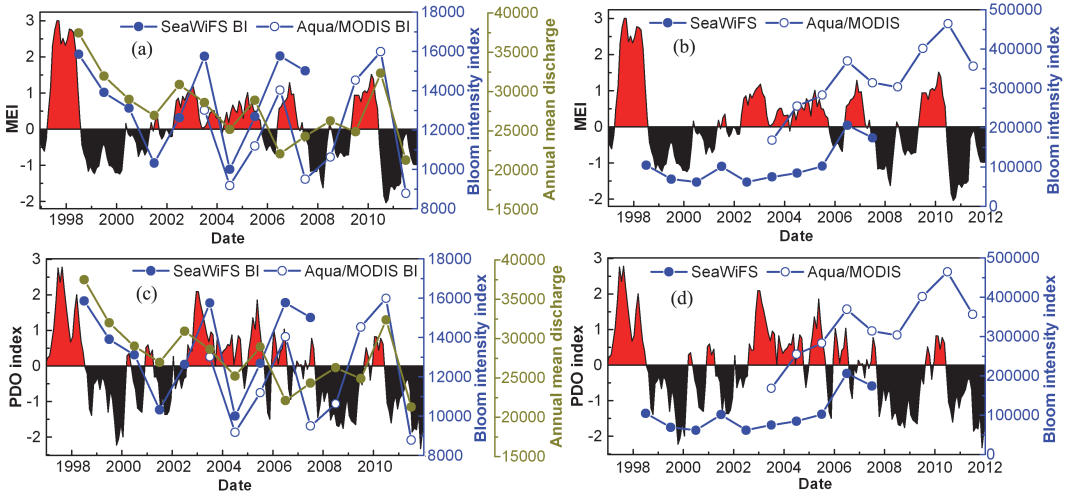

Fig. 15. Comparisons of the inter-annual variations among the bloom intensity index (BI with unit of $kg\,m^{-1}$), annual mean discharge of Changjiang ($m^3\,s^{-1}$), MEI and PDO index. **(a)** and **(b)** are the comparisons between BI and MEI at regions A and B as shown in Fig. 11a, respectively. **(c)** and **(d)** are the comparisons between BI and PDO index at regions A and B, respectively.

BGD
10, 111–155, 2013

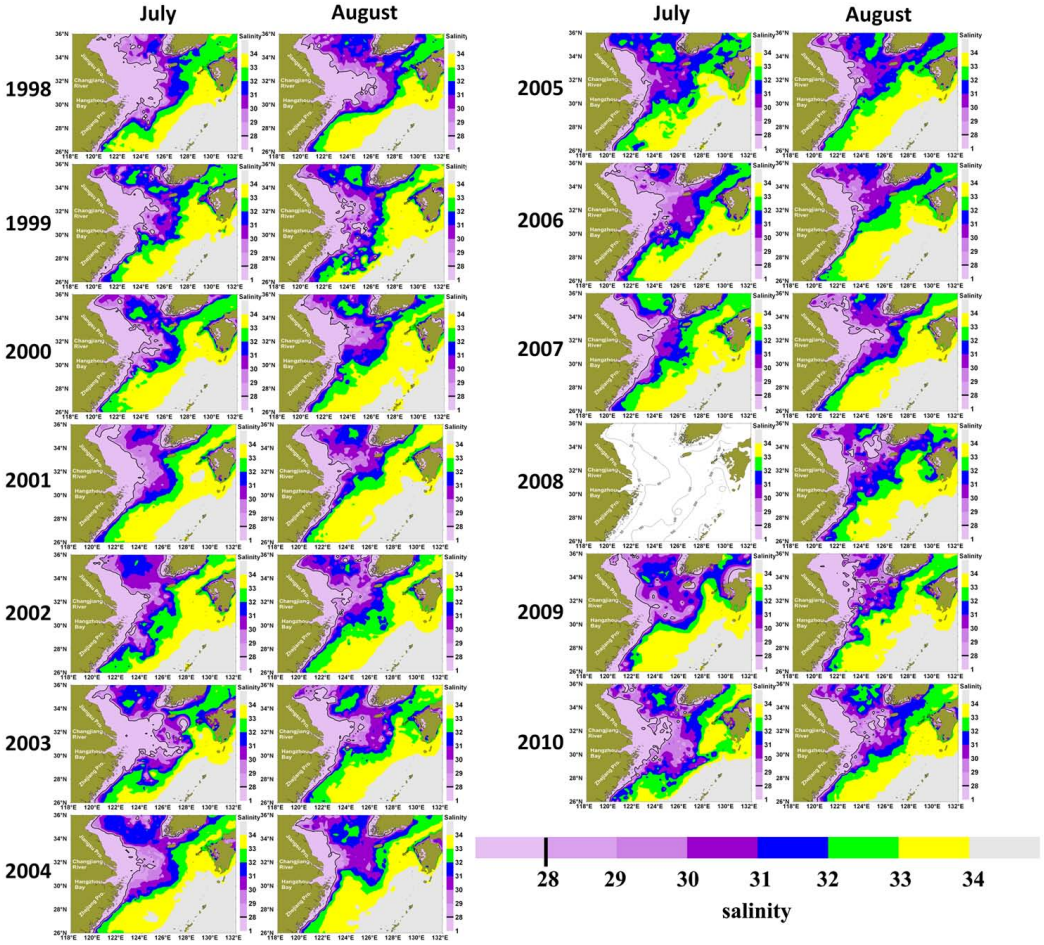

Fig. A1. SeaWiFS-derived monthly Changjiang plumes during 1998–2010 (taken from Bai et al., 2013b).

BGD
10, 111–155, 2013

Variability of phytoplankton blooms in the eastern China seas

X. Q. He et al.